BIOCHEMISTRY
including biophysical chemistry & molecular biology
Article

Biochemistry **2011,** *50,* 989–1000 989
DOI: 10.1021/bi101795q

Structure and Interactions of Plant Cell-Wall Polysaccharides by Two- and Three-Dimensional Magic-Angle-Spinning Solid-State NMR†

Marilú Dick-Pérez,‡ Yuan Zhang,‡ Jennifer Hayes,‡,∥ Andre Salazar,§ Olga A. Zabotina,*,§ and Mei Hong*,‡

‡*Department of Chemistry and Ames Laboratory and* §*Department of Biochemistry, Biophysics, and Molecular Biology, Iowa State University, Ames, Iowa 50011, United States.* ∥*Current address: Torrington High School, Torrington, WY 82240.*

Received November 9, 2010; Revised Manuscript Received December 30, 2010

ABSTRACT: The polysaccharide-rich cell walls (CWs) of plants perform essential functions such as maintaining tensile strength and allowing plant growth. Using two- and three-dimensional magic-angle-spinning (MAS) solid-state NMR and uniformly ^{13}C-labeled *Arabidopsis thaliana*, we have assigned the resonances of the major polysaccharides in the intact and insoluble primary CW and determined the intermolecular contacts and dynamics of cellulose, hemicelluloses, and pectins. Cellulose microfibrils showed extensive interactions with pectins, while the main hemicellulose, xyloglucan, exhibited few cellulose cross-peaks, suggesting limited entrapment in the microfibrils rather than extensive surface coating. Site-resolved ^{13}C T_1 and ^{1}H $T_{1\rho}$ relaxation times indicate that the entrapped xyloglucan has motional properties that are intermediate between the rigid cellulose and the dynamic pectins. Xyloglucan absence in a triple knockout mutant caused the polysaccharides to undergo much faster motions than in the wild-type CW. These results suggest that load bearing in plant CWs is accomplished by a single network of all three types of polysaccharides instead of a cellulose−xyloglucan network, thus revising the existing paradigm of CW structure. The extensive pectin−cellulose interaction suggests a central role for pectins in maintaining the structure and function of plant CWs. This study demonstrates the power of multidimensional MAS NMR for molecular level investigation of the structure and dynamics of complex and energy-rich plant materials.

The cell walls of higher plants are responsible for the mechanical strength, tissue cohesion, ion exchange, protection against biotic and abiotic stresses, and growth and division of plant cells. While plant CWs[1] have long been used in the paper and textile industry, they recently gained further economic importance as the source of lignocellulose-based biofuels due to their high content of energy-rich polysaccharides. A comprehensive understanding of the structure, intermolecular interactions, and dynamics of polysaccharides in CWs thus has both fundamental and practical importance (*1*).

Two distinct layers of wall usually protect plant cells: a thin primary wall formed during plant growth and a thick secondary wall formed in cells that have completed their growth. While secondary CWs are structurally diverse and often contain lignin, the primary walls of various species of growing plants share many common features (*2*, *3*). In dicots, the primary CWs contain three major classes of polysaccharides: cellulose, whose microfibrils constitute the rigid framework of the CW; hemicelluloses, which mainly consist of xyloglucan (XG) and a small amount of glucoronoarabinoxylan; and pectins, which mainly include homogalacturonan (HG) and rhamnogalacturonan (RG) I and II (Figure 1B−H) (*4*). In addition, primary cell walls contain structural proteins and glycoproteins (*3*). While the structural role of cellulose microfibrils has been extensively studied, the molecular interactions of hemicelluloses and pectins with cellulose microfibrils have not been investigated in intact CWs (*1*). The most common structural model depicts a cellulose−hemicellulose network embedded in a pectin matrix (*5*, *6*). Such structural models were largely obtained from fractionation-based chemical analysis, biochemical studies, and electron and optical microscopies (*6*, *7*), which often altered or destroyed the physicochemical properties of the polysaccharides of interest. For example, alkaline extraction deacetylates hemicelluloses, changes their interaction with cellulose, and converts cellulose I to cellulose II (*8*, *9*). Microscopic techniques emphasize the crystalline cellulose and are poorly suited for detecting the amorphous noncellulosic polysaccharides (*7*).

High-resolution magic-angle-spinning (MAS) solid-state NMR spectroscopy probes the atomic and molecular structures of insoluble macromolecules and has been used to investigate the structures of various allomorphs of cellulose (*10*, *11*) and cellulose−hemicellulose composites (*12*, *13*). However, due to the low sensitivity of ^{13}C NMR of naturally abundant material, multidimensional correlation solid-state NMR, which is now widely used for structure determination of membrane proteins and fibrous proteins (*14*−*16*), has not been used to elucidate the molecular structure of CW polysaccharides.

In this work we demonstrate the first application of two- and three-dimensional MAS ^{13}C correlation NMR spectroscopy to

†This work was supported by the U.S. Department of Energy, Office of Basic Energy Sciences, Division of Materials Sciences and Engineering, under Award AL-90-360-001. Initial experiments were funded by the Iowa State University Foundation.

*Corresponding authors. M.H.: tel, 515-294-3521; fax, 515-294-0105; e-mail, mhong@iastate.edu. O.A.Z.: tel, 515-294-6125; e-mail, zabotina@iastate.edu.

[1]Abbreviations: CW, cell wall; XG, xyloglucan; HG, homogalacturonan; RG, rhamnogalacturonan; Ara, arabinose; Rha, rhamnose; Gal, galactose; Xyl, xylose; Glc, glucose; CP, cross-polarization; DP, direct polarization; DQF, double quantum filtered; SQ, single quantum; DIPSHIFT, dipolar chemical shift correlation; DARR, dipolar-assisted rotational resonance; MAS, magic angle spinning.

Published on Web 01/04/2011

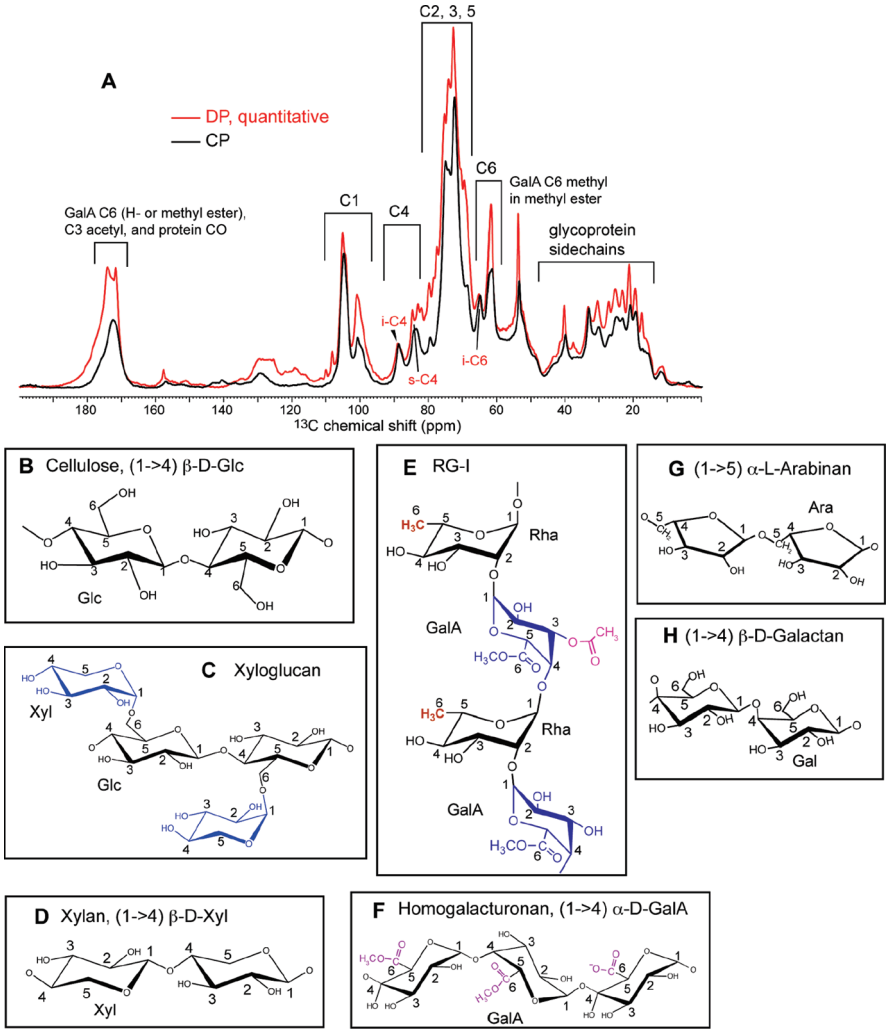

FIGURE 1: 1D ^{13}C MAS spectra and chemical structures of the main polysaccharides of *Arabidopsis* primary CWs. (A) ^{13}C spectra measured using ^{13}C CP (black) and DP with a 25 s recycle delay to obtain quantitative intensities (red). The interior cellulose C4 signal at 88 ppm is the highest CP signal that matches with the DP signal, indicating interior cellulose is the most rigid polysaccharide of the CW. The spectral regions for different carbons of the hexose sugars are indicated, and a few well-resolved cellulose peaks are assigned. (B−H) Chemical structures of the main polysaccharides in *Arabidopsis* primary CW: (B) cellulose; (C) xyloglucan; (D) xylan; (E) RG-I; (F) homogalacturonan; (G) arabinan; (H) galactan.

the primary CWs of plants. Uniform ^{13}C labeling of *Arabidopsis thaliana*, a well-characterized dicotyledonous plant (*4*), provided the sensitivity necessary for correlation-based assignment of the polysaccharide chemical shifts and extraction of 3D structural information of the primary CWs. We show that even with the complexity and heterogeneity of the intact CW it is possible to extract intermolecular cross-peaks among different polysaccharides using 3D ^{13}C NMR. Combined with data on an XG-depleted mutant *Arabidopsis* CW, we obtained new insights into the nature and extent of interactions among the three major classes of polysaccharides and propose a revised model of the CW architecture.

MATERIALS AND METHODS

Plant Material. Two types of *A. thaliana* plant CWs were examined in this study: the wild-type and a *xxt1xxt2xxt5* triple knockout line. The latter was generated by crossing homozygous *xxt1xxt2* (*17*) and *xxt2xxt5* (*18*) double knockout lines and was confirmed by a PCR screen. The *xxt1xxt2* double mutant was previously reported to have no detectable xyloglucan (XG) content (*17*), while the *xxt5* single mutant had significant reduction of XG (*18*). The triple knockout mutant has drastically reduced amounts of glycosyl residues typically assigned to XG, such as 4,6-Glc, t-Xyl, and 2-Gal (Table 1), confirming the lack of XG.

Wild-type and homozygous *xxt1xxt2xxt5* mutant plants were germinated and grown at 21 °C in the dark in a liquid culture with uniformly ^{13}C labeled glucose as the only carbon source (5 g/L). The culture was shaken at 130 rpm. After 14 days, whole seedlings, including roots and hypocotyls, were powdered in liquid nitrogen and mixed with 80% ethanol (v/v). The mixture was heated for 1 h at 80 °C, cooled to room temperature, and homogenized using Polytron at the highest speed for 2 min. The homogenate was centrifuged at 12000*g* for 20 min. The ethanol supernatant containing small cytoplasmic molecules was decanted. The pellet was resuspended in a chloroform : methanol (1:1) solution, shaken for 30 min, and centrifuged at 12000*g* for 20 min to remove lipids and other nonpolar compounds. The pellet was then washed three times with acetone and air-dried. Dry alcohol-insoluble residues were resuspended in 50 mM sodium acetate buffer (pH 5.2) containing 1.5% of sodium dodecyl sulfate (SDS) and 5 mM sodium metabisulfate. The mixture was shaken overnight and centrifuged. This step removed most of the intracellular proteins, soluble CW proteins, and low molecular

Table 1: Glycosyl Residue Linkage Analysis of Wild-Type and Mutant *Arabidopsis* CW Polysaccharides[a]

glycoside linkage	wild type (mol %)	*xxt1xxt2xxt5* (mol %)
t-Fuc	**1.2**	**0.1**
t-Rha	1.5	2.4
2-Rha	4.6	5.3
2,4-Rha	*2.3*	*4.0*
t-Ara	7.3	8.8
2-Ara	2.3	2.3
3-Ara	*6.1*	*3.6*
5-Ara	*5.8*	*11.3*
t-Xyl	**11.4**	**5.8**
2-Xyl	**2.7**	**1.8**
4-Xyl	*5.3*	*9.0*
2,4-Xyl	1.3	1.9
t-Gal	5.8	5.5
2-Gal	**5.0**	**1.6**
4-Gal	8.7	9.4
4,6-Gal	0.7	0.9
t-Glc	5.1	5.1
3-Glc	2.9	3.4
4-Glc	**4.6**	**2.8**
6-Glc	0.7	1.0
4,6-Glc	**7.5**	**1.5**
t-Man	1.0	1.0
4-Man	*2.6*	*5.9*
4,6-Man	2.1	3.7
residue		
Fuc	1.5	0.1
Rha	9.3	11.9
Ara	*15.5*	*19.0*
Xyl	*23.3*	*19.0*
Gal	16.6	14.3
Glc	18.9	16.7
Man	*4.5*	*8.2*
GalA	8.3	8.7
GlcA	2.2	2.1

[a]Bold indicates the mol % of XG residues, and italic underline indicates other residues that show significant percentage changes.

weight compounds. The pellet was washed several times with 50 mM sodium acetate buffer to remove SDS. Solids were resuspended in the same buffer containing 5 units of α-amylase (from *Bacillus* species, 3100 units/mg; Sigma) and 0.01% thimerosal, and the mixture was incubated while shaking for 48 h at 25 °C. This step digested and removed starch, which comes from starch-containing plastids in the cell and is unrelated to the CW. The pellet containing purified CW material was washed with water to remove the digested starch, washed with acetone, and air-dried.

About 30 mg of CW material was dialyzed against water for 2 days at 4 °C. The CW material was lyophilized and rehydrated to 45% (w/w) by phosphate buffer (pH 7.5). The hydrated mixture was vortexed for 10 min to homogenize the sample and packed into NMR rotors.

Glycosyl Residue Linkage Analysis. Five milligrams of lyophilized CW material was methylated according to a modified protocol of Ciucanu (*19*). Permethylated carbohydrates were hydrolyzed by 2 M trifluoroacetic acid and further derivatized into the corresponding alditol acetates (PMAA) with $NaBD_4$ as the reducing agent. The resulting mixture of PMAA was analyzed by gas chromatography−mass spectrometry using a 30 m × 0.25 mm (i.d.) SP-2330 capillary column (Supelco) and gas chromatograph (Agilent) coupled to a mass spectrometer. Glycoside identity and linkage types were determined by their corresponding retention times, which were measured by running PMAA of commercially available polysaccharides. The mole percentage composition of the samples was calculated by normalizing the chromatogram peak areas to the molecular masses of the corresponding derivatives (*18*). To differentiate between 2-Xyl and 4-Xyl, the mass difference of the primary ions resulting from the deuterium introduced at the C-1 position during reduction by $NaBD_4$ was taken into account. Analyses of linkage composition were performed on five CW preparations from separately grown plants.

Solid-State NMR. Most MAS NMR spectra were measured on a Bruker Avance 600 (14.1 T) spectrometer operating at resonance frequencies of 600.13 MHz for ^{1}H and 150.9 MHz for ^{13}C. A double-resonance 4 mm MAS probe was used. 2D ^{13}C double-quantum-filtered (DQF) experiments were carried out on a Bruker Avance II 700 MHz (16.5 T) spectrometer using a 3.2 mm MAS probe. Typical radio-frequency (rf) field strengths were 62 kHz for ^{1}H decoupling and 5 μs for the ^{13}C 90° pulses. MAS frequencies ranged from 7 to 12 kHz (Supporting Information Table S4). ^{13}C chemical shifts were referenced to the ^{13}CO signal of α-glycine at 176.49 ppm on the TMS scale.

The pulse sequences used to acquire the 2D and 3D ^{13}C spectra are given in Supporting Information Figure S1. Initial transverse ^{13}C magnetization was created by ^{1}H−^{13}C cross-polarization (CP) for experiments that preferentially detected rigid polysaccharides and by ^{13}C direct polarization (DP) for experiments that enhanced the signals of mobile polysaccharides. Recycle delays ranged from 1.5 to 25 s. The long recycle delays were used in experiments that aimed to give quantitative intensities.

The 2D DQF correlation experiment used the SPC5 sequence (*20*) to recouple the ^{13}C−^{13}C dipolar interaction under MAS (Supporting Information Figure S1A). The 2D spin diffusion experiment, either with ^{1}H irradiation under the DARR condition (*21*) or without, was conducted using mixing times from 5 to 300 ms (Supporting Information Figure S1B). The 2D INADEQUATE experiment used ^{13}C DP excitation, ^{13}C−^{13}C *J*-coupling for polarization transfer (*22*), and a short recycle delay of 2 s (Supporting Information Figure S1C) to enhance the signals of mobile polysaccharides. The 3D CCC correlation experiment (Supporting Information Figure S1D) contained two spin-diffusion mixing periods, t_{m1} and t_{m2}, where t_{m1} is short (≤8 ms) and t_{m2} can be either short (5 ms) or long (100−300 ms) (*23*). The long t_{m2} allowed the observation of both intramolecular and intermolecular correlation peaks while the short t_{m2} detected only intramolecular correlations. Chemical shift assignment was made using the software Sparky 3 (T. D. Goddard and D. G. Kneller, University of California, San Francisco).

The undoubled version of the 2D dipolar chemical shift (*24*) correlation (DIPSHIFT) experiment was used to measure ^{13}C−^{1}H dipolar couplings site-specifically. The experiment was conducted under 7 kHz MAS, and ^{1}H homonuclear decoupling was achieved using the frequency-switched Lee−Goldburg (FSLG) sequence (*25*). The FSLG-scaled rigid-limit one-bond ^{13}C−^{1}H dipolar coupling was measured on the crystalline model peptide formyl-Met-Leu-Phe to be 13.0 kHz. This value was confirmed by experiments at 243 K where the polysaccharide motion was frozen. Bond order parameters were calculated as the ratio of the observed couplings with the rigid-limit value (Supporting Information Table S1).

^{13}C T_1 relaxation times were measured using the inversion recovery experiment $\pi(^{13}C)-\tau-\pi/2(^{13}C)-$acquire. Direct ^{13}C polarization was used in combination with long recycle delays

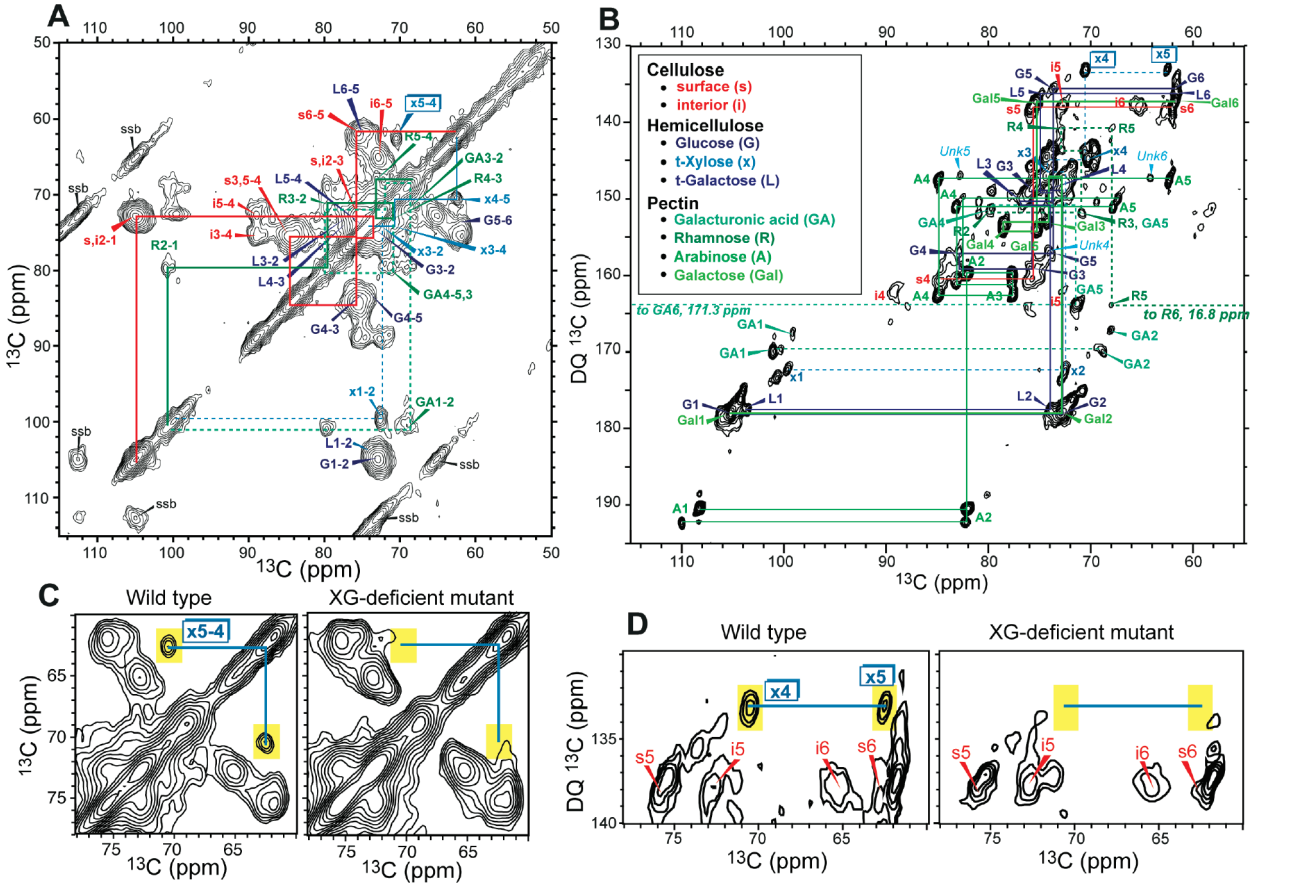

FIGURE 2: 2D ^{13}C correlation spectra of *Arabidopsis* primary CWs for resonance assignment of the polysaccharides. (A) 2D DQF spectrum of wild-type CWs showing one-bond correlations. (B) 2D INADEQUATE spectrum of wild-type CWs to preferentially detect the signals of mobile polysaccharides. Color code and abbreviations for assignments are given in the inset. (C) Comparison of the DQF spectra of wild-type and XG-deficient mutant CWs. The Xyl C5−C4 cross-peak is absent in the mutant spectrum. (D) Comparison of wild-type and mutant INADEQUATE spectra, confirming the absence of Xyl signals.

to ensure quantitative signal intensities. The recycle delay was 15 s for the wild-type sample and 10 s for the mutant CW sample.

Spin-diffusion-free ^{1}H $T_{1\rho}$ relaxation times were measured via ^{13}C detection using the pulse sequence $\pi/2(^{1}H)-^{1}H$ LG-SL-$(\tau)-^{1}H-^{13}C$ LG-CP−acquire. The Lee−Goldburg (LG) spin lock and LG-CP periods, by suppressing ^{1}H spin diffusion, ensure that the measured relaxation times are specifically of the protons directly bonded to the observed ^{13}C spin. The relaxation data were fit using the software KaleidaGraph. Most relaxation curves required double-exponential fits (Tables 3 and 4).

RESULTS

Resonance Assignment of CW Polysaccharides by 2D and 3D MAS NMR. We produced uniformly ^{13}C-labeled cell walls by germinating and growing wild-type and XG-deficient *Arabidopsis* plants in the dark in liquid culture supplemented with uniformly ^{13}C-labeled glucose (Glc). Cell walls were isolated from 14-day-old etiolated seedlings, including roots and hypocotyls (*26*). Since all tissues of the plant were used for the NMR samples, the structural information obtained here represents the average composition of the entire plant's primary CWs. In young growing seedlings, secondary cell walls are present only in the cells of specialized vascular tissues and represent only a small portion of the total CW preparation. All insoluble CW components, including structural glycoproteins and polysaccharides, were retained, while soluble proteins were extracted by treatment with SDS. Usually, primary CWs contain a low amount of structural glycoproteins, the majority of which are arabinogalactan proteins with carbohydrate side chains composed of 1,6-Gal and 1,3-Ara (*3*).

Figure 1A shows 1D ^{13}C MAS spectra of wild-type *Arabidopsis* primary CWs. Both polysaccharide and glycoprotein signals were observed in their characteristic spectral ranges of 60−110 and 10−60 ppm, respectively. The major sugar ^{13}C signal regions were approximately indicated based on literature ^{13}C chemical shifts of cellulose and other purified CW components (*10*). Figure 1B−H displays the chemical structures and nomenclature for the most common polysaccharides of the primary CWs. Two ^{13}C spectra are shown in Figure 1A. One was measured using ^{13}C DP and a long recycle delay of 25 s so that the intensities quantitatively reflect the relative amounts of the various CW components. A second spectrum was measured using $^{1}H-^{13}C$ CP (*27*), which preferentially enhances the signals of rigid components due to their strong $^{1}H-^{13}C$ dipolar couplings. The intensities of the two spectra were scaled such that the highest intensity in the CP spectrum equals but does not exceed the corresponding DP intensity. This criterion placed the 89 ppm peak, which is the C4 signal of crystalline cellulose of the microfibril interior, to be equal between the DP and CP spectra. All other ^{13}C signals were enhanced in the quantitative DP spectrum. Thus, the interior of the cellulose microfibril is the most rigid species among all CW components, as expected.

The high sensitivity afforded by ^{13}C-labeling of the CWs made it possible to measure 2D and 3D correlation NMR spectra to

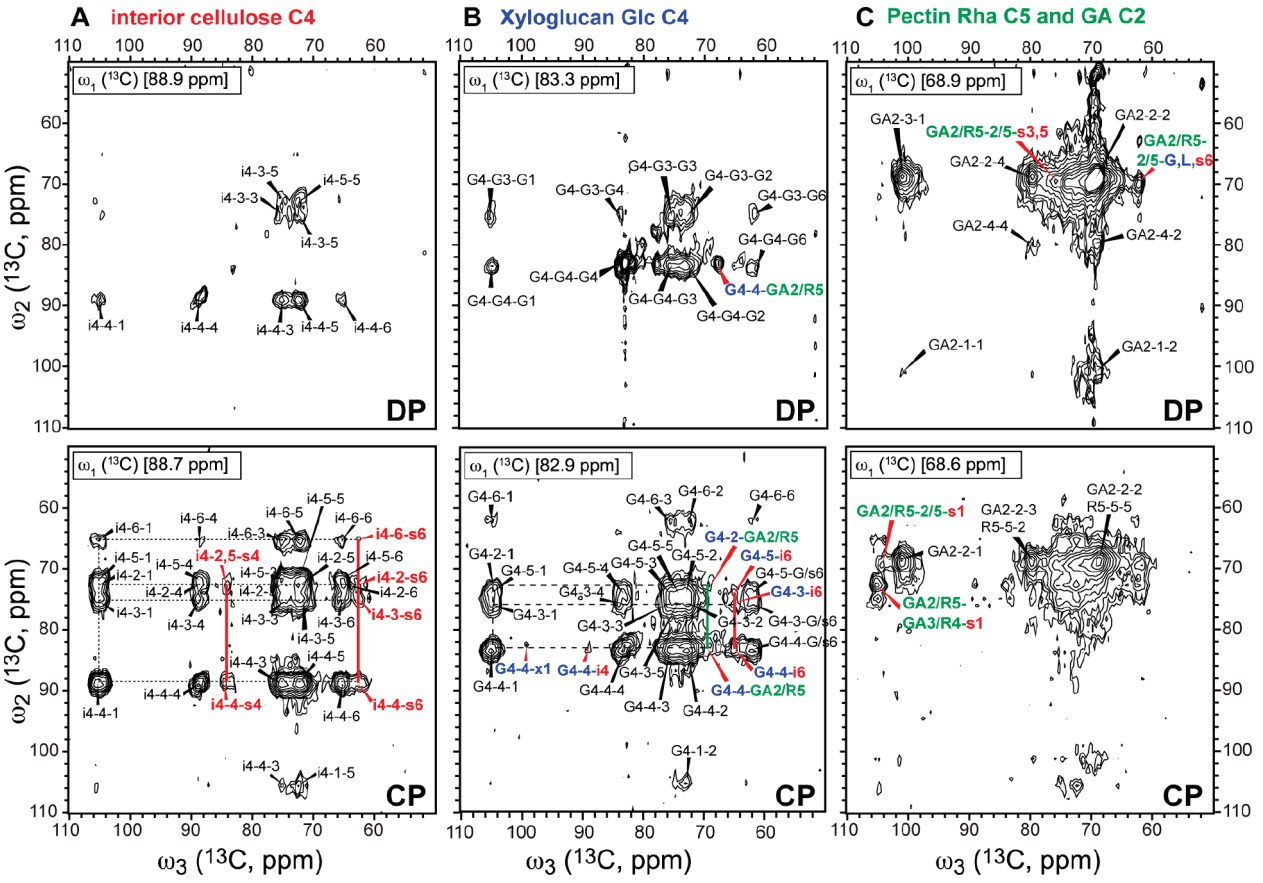

FIGURE 3: Selected 2D planes of 3D CCC spectra of wild-type CWs measured with DP (t_{m2} = 100 ms, top) and CP (t_{m2} = 300 ms, bottom) to preferentially detect the signals of mobile and rigid polysaccharides, respectively. (A) 89 ppm plane of interior cellulose C4. (B) 83 ppm plane of XG glucose C4. (C) 68.9 ppm plane of Rha C5 and GA C2. Intermolecular cross-peaks are assigned in color.

resolve the highly overlapping ^{13}C signals in the 1D spectra and to identify intermolecular contacts. Figure 2 shows two 2D ^{13}C−^{13}C correlation spectra that allowed partial assignment of both rigid and mobile polysaccharides. A ^{13}C double-quantum-filtered (DQF) correlation experiment using ^{13}C−^{13}C dipolar couplings for polarization transfer yielded mostly one-bond cross-peaks of rigid polysaccharides (Figure 2A). In all spectra shown in this paper, we annotate the cellulose resonances in red, hemicellulose signals in various shades of blue, and pectin signals in shades of green. Strong cellulose cross-peaks such as C1−C2 were readily identified, and signals of interior versus surface cellulose were distinguished in the 85−89 ppm (C4) and 62−65 ppm (C6) ranges. In assigning the spectra, we used the literature chemical shifts of purified CW polysaccharides to facilitate the connectivity-based "walk" of the 2D spectra (Supporting Information Figure S2A). The lack of multiple-bond correlation peaks in the 2D DQF spectrum simplified the assignment. We also measured 2D spin diffusion ^{13}C correlation spectra with varying mixing times (Supporting Information Figure S3A) to obtain multiple-bond cross-peaks such as C1−C3 and C1−C4, which confirmed the assignments of the 2D DQF spectrum. The spin diffusion spectra also showed additional broad and low-intensity signals from galacturonic acid (GA) and rhamnose (Rha) in pectic polysaccharides such as RG and HG (*28*), suggesting that pectins are more mobile than cellulose, which suppressed their signals in the 2D DQF spectrum.

Solid-state NMR provides a number of techniques to distinguish rigid and mobile molecules in a complex mixture, not only by using CP or DP to create the initial magnetization but also by using suitable polarization transfer schemes and recycle delays. The 2D DQF spectrum in Figure 2A was measured using CP and thus enhanced the signals of rigid polysaccharides. To maximally observe the signals of mobile CW polysaccharides, we conducted a DP 2D J-INADEQUATE experiment where double-quantum (DQ) ^{13}C coherence was excited using ^{13}C−^{13}C through-bond *J*-coupling and correlated with single-quantum (SQ) signals (*22*) (Supporting Information Figure S1C). The use of *J*-coupling rather than dipolar coupling, a short recycle delay, and direct ^{13}C excitation combined to enhance the signals of mobile polysaccharides. Moreover, the INADEQUATE spectrum by design does not have diagonal peaks; thus it is particularly effective in resolving peaks with similar chemical shifts, which were obscured in the spin diffusion and DQF spectra (*22*). The resulting 2D spectrum of wild-type CW (Figure 2B) showed that most cellulose signals except for the mobile C6 were much attenuated, and new sharp signals with line widths of 0.4−0.8 ppm appeared that were either absent or unresolved in the dipolar-based 2D DQF and spin diffusion spectra. These sharp resonances were assigned to arabinose (Ara) (*29*), galactose (Gal), Rha, and GA in pectins and to galactose (L) and xylose (Xyl) in hemicellulose side chains (*30*) based on the connectivity patterns (Supporting Information Figure S2B) and by comparison with literature (Supporting Information Table S5). Galactose is found in both pectins and hemicellulose and is denoted as Gal for the pectin portion and L for the hemicellulose side chains. For the pectic sugars Ara and Gal, all ^{13}C resonances of each ring were found in the INADEQUATE spectra, indicating the dynamic nature of the pectin side chains. For Rha, the C1−C2 cross-peaks are

missing, which is consistent with the fact that these two carbons participate in the glycosidic linkages of the RG backbone and is thus much more rigid. Therefore, the INADQUATE spectrum is an accurate reporter of the dynamic environment of the polysaccharides.

Table 2: ^{13}C Chemical Shifts (ppm) of Polysaccharides in Wild-Type *Arabidopsis* Primary CWs

sites	C1	C2	C3	C4	C5	C6
cellulose						
surface (s)	105.0	72.7	75.3	85.0	75.3	62.5
interior (i)	105.0	72.7	75.5	88.8	72.0	65.2
pectin						
RG I, 1,2-Rha (R)	101.0	79.7	71.1	72.9	68.1	16.8
RG I, Ara (A)	108.2	82.0	77.6	84.9	62.3	
	110.0			82.5	67.3	
				83.2	67.8	
HGA/RG I, GalA (GA)	101.0, 99.0	69.0, 68.0	72.0	80.0	71.4	171.3
galactan, Gal	105.0	72.6	74.3	78.4	75.2	61.7
hemicellulose						
xyloglucan 1,4-Glc (G)	105.0	72.7	75.9	83.0	73.8	61.5
xyloglucan t-Gal (L)	104.0	74.0	76.7		74.8	61.7
xyloglucan t-Xyl (x)	99.7	72.5	74.4	70.5	62.3	
xylan 1,4-Xyl (Xn)	98.0	72.6	75.5	78.5	63.0	

While these 2D spectra allowed the identification of many polysaccharide signals, spectral congestion still made it difficult to fully resolve and assign all polysaccharide signals. More importantly, the resonance overlap made it difficult to determine intermolecular cross-peaks that are indicative of close spatial contacts. To enhance the spectral resolution of the CW samples, we conducted 3D ^{13}C−^{13}C−^{13}C correlation experiments (*23*) in which the first and second dimensions correlated carbons in the same molecule via a short mixing time, t_{m1} (5−8 ms), while the second and third dimensions potentially correlated carbons in

We carried out the same 2D experiments on the XG-deficient mutant CW, and the resulting spectra confirmed the absence of xyloglucan. For example, the Xyl C4−C5 cross-peak, which was well resolved from other signals in the wild-type CW spectra, was conspicuously missing in the DQF and INADEQUATE spectra of the mutant (Figure 2C,D). Various Glc signals of XG backbone were also suppressed or weakened (Supporting Information Figure S3B,C). The absence of XG signals is consistent with glycosyl residue linkage analysis of the XG-deficient mutant (Table 1), which showed significant reduction of t-Xyl, 2-Xyl, 2-Gal, and 4,6-Glc, which are residues typically assigned to XG. Since these glycosyl residues can also be found in other polysaccharides, they were still detected in small quantities in the XG-deficient mutant.

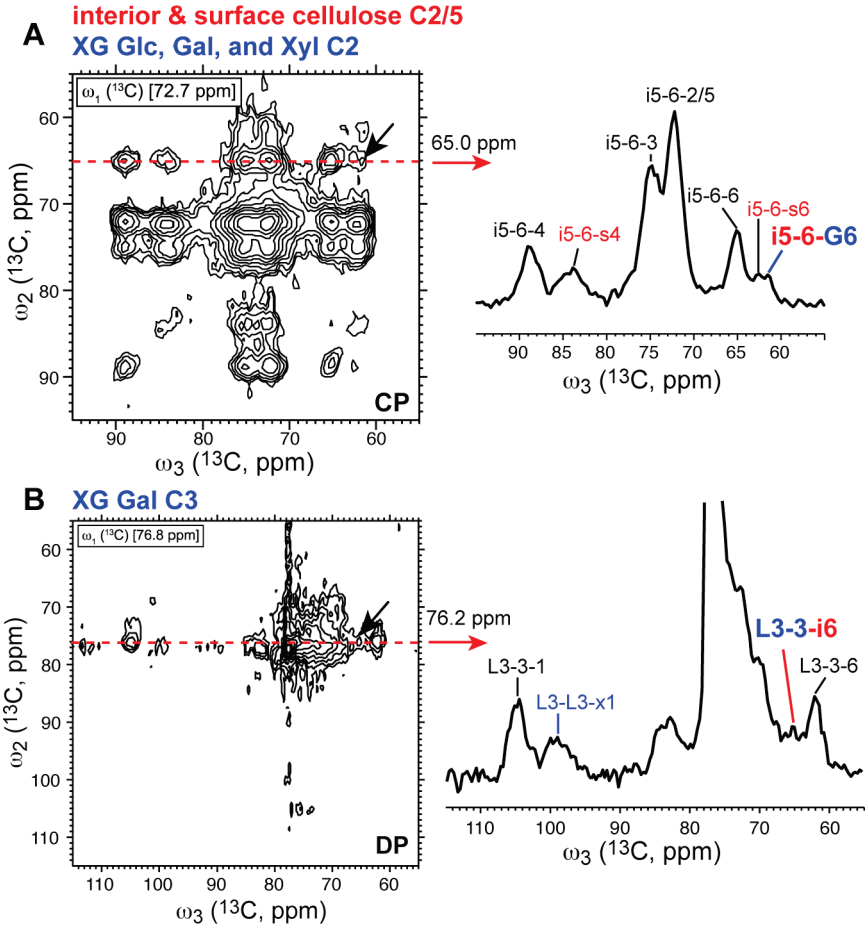

FIGURE 4: Additional hemicellulose−cellulose cross-peaks from 3D CCC spectra. (A) 72.7 ppm ω_1 plane of the CP-CCC spectrum with t_{m2} = 300 ms. The ω_2 cross section at 65.0 ppm, assigned to the interior cellulose C6, shows a cross-peak with the Glc C6 of XG at 61.5 ppm. (B) 76.8 ppm ω_1 plane of the DP-CCC spectrum with t_{m2} = 100 ms. The 76.2 ppm ω_2 cross section of galactose C3 of XG shows a cross-peak with interior cellulose C6.

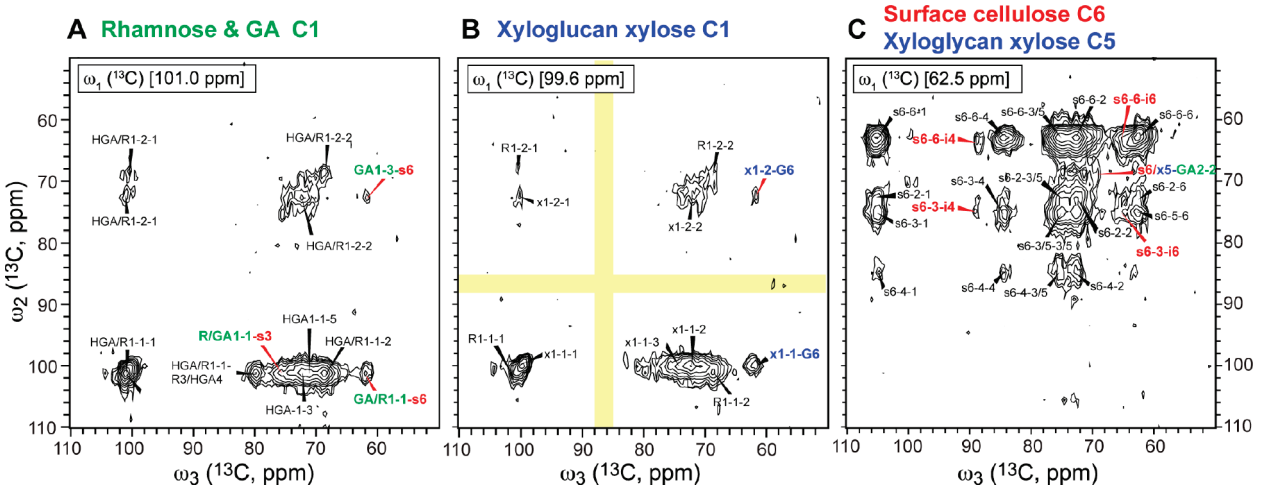

FIGURE 5: Additional ω_1 planes of the 3D CP-CCC spectrum of wild-type *Arabidopsis* CW polysaccharides. The spectrum was measured with t_{m2} = 300 ms. (A) 101.0 ppm ω_1 plane of rhamnose and GA C1. Several pectin−cellulose cross-peaks were observed. (B) 99.6 ppm ω_1 plane of xylose C1 of XG. Yellow regions indicate the absence of cross-peaks with cellulose C4. (C) 62.5 ppm ω_1 plane of surface cellulose C6 or xylose C5. A cross-peak between surface cellulose or hemicellulose and pectin was detected.

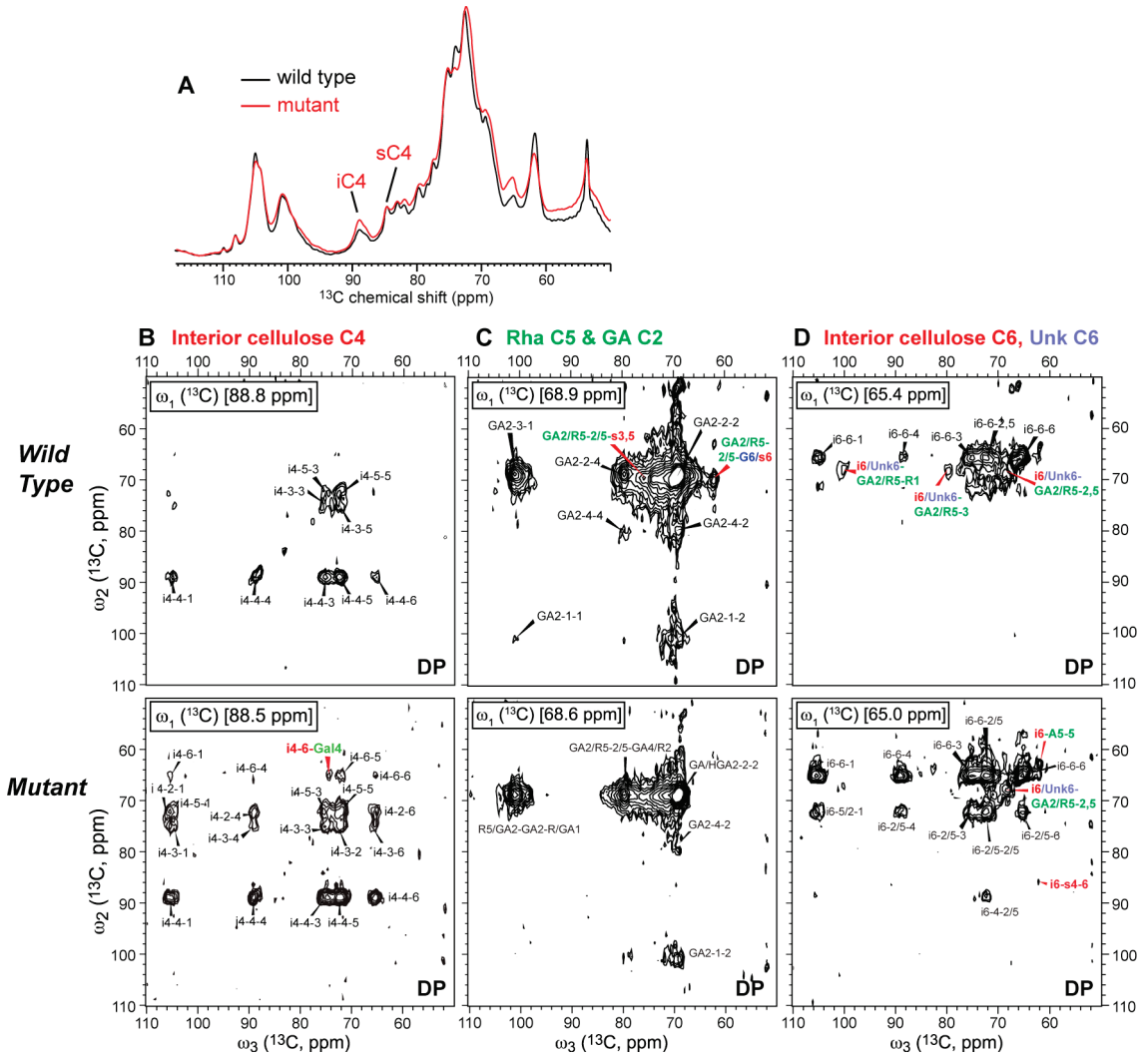

FIGURE 6: Comparison of wild-type and XG-deficient mutant *Arabidopsis* CW spectra. (A) Quantitative 1D ^{13}C DP spectra measured with long recycle delays: wild-type sample, black; mutant, red. The interior cellulose C4 signal is higher relative to the surface C4 signal in the mutant compared to the wild-type CWs. (B−D) Representative ω_1 planes of 3D DP-CCC spectra of wild-type (top) and mutant (bottom) CWs. Mixing times: t_{m1} = 5 ms; t_{m2} = 100 ms. (B) 89 ppm plane of interior cellulose C4. The larger number of cross-peaks in the mutant spectra is due to the increased mobility of the cellulose microfibrils. (C) 69 ppm plane of Rha C5 and GA C2. (D) 65 ppm plane of interior cellulose C6.

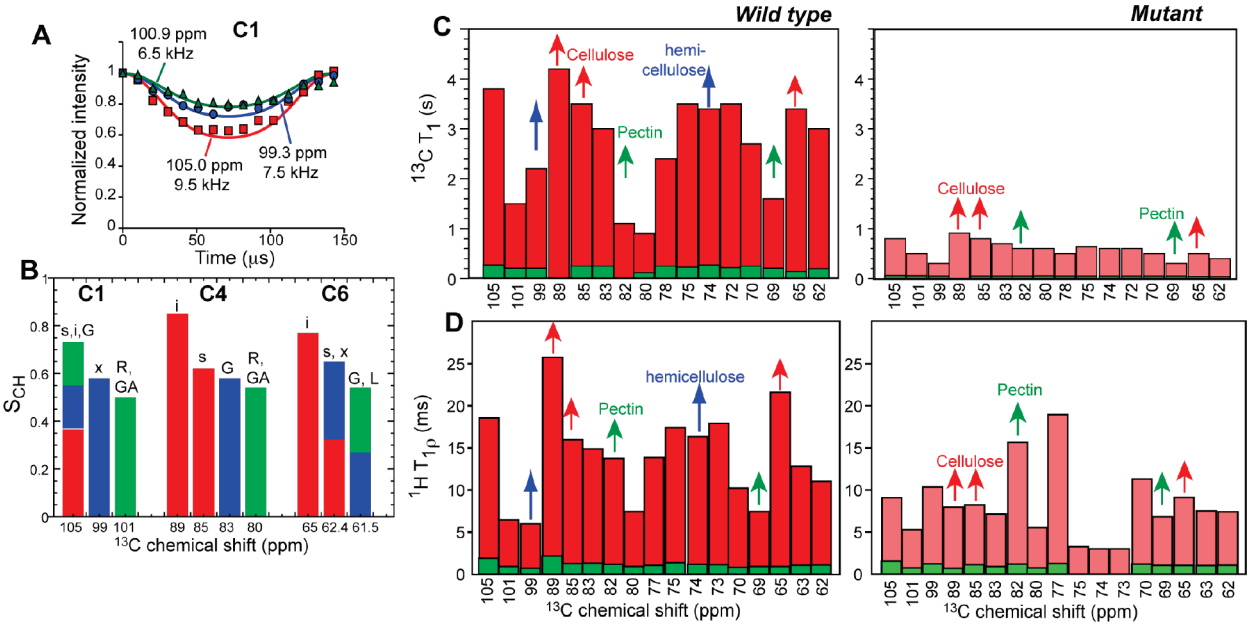

FIGURE 7: Polysaccharide dynamics in wild-type and XG-deficient mutant CWs at 293 K. (A) Representative C−H dipolar dephasing curves from quantitative 2D dipolar-shift correlation experiments. Cellulose has the largest dipolar dephasing and pectin the least. (B) Comparison of S_{CH}'s in wild-type CWs. Overlapped peaks are represented by multicolored bars, whose individual heights reflect the number of polysaccharide signals in each category. (C) ^{13}C T_1 relaxation times of wild-type (left) and mutant (right) CWs. The long and short T_1 components are indicated in red and green, respectively. (D) Site-specific ^{1}H $T_{1\rho}$ relaxation times of wild-type (left) and mutant (right) CWs.

different polysaccharides by a long mixing time, t_{m2} (Supporting Information Figure S1D). Several 3D spectra with either DP or CP excitation and with long or short t_{m2} were measured to preferentially detect dynamic or rigid polysaccharides and to enhance long-range versus short-range correlation peaks. Figure 3 shows representative ω_1 planes of 3D DP and CP spectra of wild-type CW, measured using t_{m2} of 100 and 300 ms, respectively. Additional ω_1 planes are shown in Supporting Information Figures S4 and S5. The enhanced spectral dispersion by 3D spectra allowed full assignment of the major polysaccharides, whose chemical shifts are listed in Table 2. Moreover, the 3D spectra yielded a number of intermolecular cross-peaks indicative of close spatial contacts. For example, the 89 ppm plane of interior cellulose C4 (Figure 3A) exhibited numerous cross-peaks with surface cellulose carbons such as C4 (85 ppm) and C6 (62 ppm) in the CP-CCC spectrum, indicating that the cellulose microfibrils in wild-type CWs have sufficiently small diameters to allow close packing of the surface and interior glucan chains. The same ω_1 plane exhibited fewer peaks in the DP CCC spectrum, as expected for the rigid cellulose microfibrils. In the 83 ppm plane of the XG backbone Glc C4, cross-peaks with GA and Rha were identified, indicating hemicellulose−pectin contacts. We also detected weak cross-peaks from interior cellulose to the glucan backbone (Figure 3B) and the Gal side chains of XG (Figure 4), but no cellulose−Xyl cross-peaks could be identified in the relatively resolved Xyl C1 plane at 99.6 ppm (Figure 5B). Finally, the 69 ppm plane of GA C2 and Rha C5 of pectins showed multiple cross-peaks with surface cellulose (Figure 3C); similarly, the C1 peak of Rha and GA at 101 ppm also exhibited clear cross-peaks with surface cellulose (Figure 5A). Thus, pairwise interactions among all three types of polysaccharides were observed in the 3D spectra, but XG−cellulose cross-peaks did not dominate the spectra.

To verify the polysaccharide interactions observed for the wild-type CW, we also measured the ^{13}C spectra of XG-deficient mutant CW. The spectra exhibited subtle changes of structure from the wild-type spectra. Quantitative 1D ^{13}C DP spectra showed that the resolved C4 signal of the interior cellulose is higher in the XG-deficient mutant than in the wild-type CW, suggesting that the mutant CW has thicker cellulose microfibrils than the wild-type CW (Figure 6A). Linkage analysis of the mutant indicates that, in addition to the expected reduction of XG-related glycosides, there is a modest increase of pectin glycosides such as Rha and Ara as well as other hemicellulose glycosides such as mannose and 4-Xyl (Table 1). These changes may compensate for the absence of XG by stabilizing the CW structure and mechanical properties. The linkage analysis data in Table 1 are given as relative percentages; thus, the percentage increase of some residues may be due to the dramatic reduction of XG-associated residues rather than an absolute increase of the quantity of these residues.

We measured the 3D DP-CCC spectrum of the mutant CW and compared it with the wild-type spectrum (Figure 6B-D). Despite shorter ^{13}C T_1 relaxation times for the mutant (see Figure 7), which reduced the sensitivity of long-range cross-peaks at long mixing times, the mutant CW nevertheless exhibited many correlations between pectins and surface cellulose, indicating the retention of pectin−microfibril contacts in the CW. In the 65 ppm ω_1 panel, which was assigned to interior cellulose C6, several cross-peaks were observed at ω_2 chemical shifts of 68 ppm, which are known to be pectin GA2 or R5 peaks. However, given the short t_{m1} of 5 ms between the t_1 and t_2 dimensions, intermolecular cross-peaks between the interior of the cellulose microfibril and pectin are quite unlikely. Moreover, some of these cross-peaks disappeared in the 3D spectrum of the XG-deficient mutant, strongly suggesting that 65 ppm also has contributions from XG-related sugars. Indeed, close inspection of the 2D DP-INADEQUATE spectrum (Figure 2B) revealed two well-resolved and narrow cross-peaks at 64 and 83.5 ppm, which are further connected to a peak at 73.5 ppm. Since these peaks exhibit high intensity and narrow lineshapes in the INADEQUATE spectrum, they are likely pectin or hemicelluloses. Taken together,

Table 3: Quantitative ^{13}C T_1 Relaxation Times (s) of Wild-Type *Arabidopsis* CW Polysaccharides[a]

sites	δ_C (ppm)	*a* (rigid)	*b* (mobile)	T_{1a} (s)	T_{1b} (s)
s/iC1, GC1	105.0	0.71 ± 0.05	0.29 ± 0.05	3.8 ± 0.4	0.27 ± 0.09
RC1, GAC1	100.7	0.38 ± 0.11	0.62 ± 0.11	1.5 ± 0.4	0.21 ± 0.05
xC1, GAC1	99.3	0.31 ± 0.09	0.68 ± 0.09	2.2 ± 0.7	0.21 ± 0.05
iC4	88.9	1.0		4.2 ± 0.3	
sC4, AC4	84.6	0.69 ± 0.05	0.31 ± 0.05	3.5 ± 0.4	0.25 ± 0.08
GC4	83.0	0.52 ± 0.06	0.48 ± 0.06	3.0 ± 0.4	0.25 ± 0.05
AC2	82.0	1.0		1.1 ± 0.3	
RC2, GAC4	79.7	0.61 ± 0.07	0.39 ± 0.07	0.9 ± 0.1	0.12 ± 0.03
AC3	77.3	0.38 ± 0.06	0.62 ± 0.06	2.4 ± 0.4	0.25 ± 0.04
s/iC3, sC5	75.1	0.65 ± 0.04	0.35 ± 0.04	3.5 ± 0.3	0.23 ± 0.06
xC3, GC5	73.9	0.51 ± 0.05	0.49 ± 0.05	3.4 ± 0.4	0.27 ± 0.05
s/iC2, iC5, G/xC2, GAC3	72.6	0.59 ± 0.04	0.41 ± 0.04	3.5 ± 0.4	0.22 ± 0.05
xC4	70.4	0.35 ± 0.06	0.65 ± 0.06	2.7 ± 0.6	0.25 ± 0.04
GAC2, RC5	69.4	0.35 ± 0.08	0.65 ± 0.08	1.6 ± 0.4	0.21 ± 0.04
iC6	65.3	0.67 ± 0.05	0.33 ± 0.05	3.4 ± 0.4	0.14 ± 0.06
GC6, LC6, xC5	61.7	0.44 ± 0.05	0.56 ± 0.05	3.0 ± 0.5	0.20 ± 0.04

[a]A double exponential decay $I = a(1 - 2e^{-\tau/T_{1a}}) + b(1 - 2e^{-\tau/T_{1b}})$ where $b = 1 - a$ was used to fit the data.

the 65−68 ppm cross-peaks in the 3D DP-CCC spectrum of the wild-type CW most likely result from contact between a yet unidentified hemicellulosic sugar with pectins.

Polysaccharide Dynamics in the Cell Wall. Determination of polysaccharide dynamics gave further insights into the CW structure and molecular interactions. We examined the amplitudes and rates of segmental motions of wild-type and mutant CWs through $^{13}C-^{1}H$ dipolar couplings and NMR relaxation times, respectively. Motions faster than the dipolar coupling time scale of 10^{-5} s weaken the C−H coupling by an order parameter (S_{CH}) that indicates the amplitude of motion. We measured the $^{13}C-^{1}H$ dipolar couplings site-specifically using the 2D DIP-SHIFT experiment (*24*), where ^{13}C DP and long recycle delays were employed to obtain quantitative intensities. Figure 7A shows representative $^{13}C-^{1}H$ dipolar dephasing curves of wild-type CW extracted from the 2D spectrum. The interior and surface cellulose exhibited the strongest dipolar dephasing, indicating the largest dipolar couplings (Figure 7A). The cellulose S_{CH} order parameters were as much as ∼0.85, indicating small motional amplitudes. In comparison, pectins showed much lower S_{CH}'s of ∼0.50, corresponding to large-amplitude motions. XG displayed intermediate S_{CH}'s or moderate motional amplitudes. Better separation of the C−H couplings was achieved with a 3D experiment in which two ^{13}C chemical shift dimensions were used to resolve the dipolar couplings (Supporting Information Figure S6). The spectra qualitatively confirmed the relative sizes of the dipolar couplings. The polysaccharides in the mutant CW exhibited similar S_{CH}'s as the WT sample (Supporting Information Table S1), consistent with the significant retention of tensile strength by the mutant CW (*17*), suggesting that the packing density of the polysaccharides is similar in the mutant and wild-type CWs.

We examined the rates of polysaccharide motions using ^{13}C T_1 and ^{1}H $T_{1\rho}$ relaxation times. ^{13}C T_1 is sensitive to nanosecond motions of individual sugar units while ^{1}H $T_{1\rho}$ probes cooperative motions of the polysaccharide chains on the microsecond time scale. The ^{13}C T_1 measurement was quantitative by using DP and long recycle delays. In the wild-type CW, most polysaccharides exhibited two T_1 components, an ultrashort ^{13}C T_1 of 0.1−0.3 s common to all molecules, which give rise to a fast initial rise, and a long T_1 component that varies for different polysaccharides (Supporting Information Figure S7). The average long T_1 was 1.5 s for pectins, but much longer (3.7 s) for cellulose, while hemicelluloses exhibited an intermediate average T_1 of 2.9 s (Figure 7C). The fractions of the short and long T_1 components differed among the polysaccharides. Cellulose was dominated (∼70%) by the long T_1 component whereas pectins mainly (∼70%) exhibited the short T_1 component (Table 3). The 89 ppm signal, which is purely due to interior cellulose C4, showed a single-exponential decay of 4.2 s, indicating slow motion. For comparison, the 82 ppm signal, which is largely due to Ara C2 but with possible residual overlap from Glc C4 in XG, exhibited a single-exponential decay with a time constant of 1.1 s, indicating fast motion. The fact that these resolved peaks exhibited single-exponential decays indicates that the core of cellulose microfibrils has little nanosecond time scale motion, while RGs and HGs undergo fast segmental motions. Since pectins contain the highest fraction of the short T_1 component while interior cellulose has none, the presence of ∼30% fast-relaxing component in surface cellulose may be partly due to ^{13}C spin diffusion from pectins, which is consistent with the presence of many pectin cross-peaks to surface cellulose in the 3D spectra. The absence of the ultrashort T_1 component for interior cellulose C4 further supports the notion that pectin interaction with cellulose does not extend to the microfibril interior but is restricted to the microfibril surface.

Since ^{13}C T_1 relaxation times are influenced by spin diffusion, we measured the ^{1}H $T_{1\rho}$ relaxation times in a site-specific fashion using Lee−Goldburg spin lock (*31*). The resulting ^{1}H $T_{1\rho}$ values mirrored the ^{13}C T_1 trend to a large extent, in that the $T_{1\rho}$'s are heterogeneous and cellulose exhibited the longest $T_{1\rho}$'s and pectin the shortest (Figure 7D, Table 4). Therefore, on both the nanosecond and microsecond time scales, cellulose is the most rigid polysaccharide while pectins are the most dynamic.

Interestingly, the XG-deficient mutant showed an approximately 5-fold reduction of ^{13}C T_1's for all polysaccharides and also shorter ^{1}H $T_{1\rho}$'s (Figure 7C,D and Supporting Information Tables S2 and S3), indicating enhanced mobility of the mutant polysaccharides on both time scales. Cellulose had the largest $T_{1\rho}$ reduction, indicating that the rates of microfibril motion increased from the slow side of the relaxation curve (with long $T_{1\rho}$'s) to near the minimum (short $T_{1\rho}$'s). Taken together, these relaxation data indicate that the suppression of XG synthesis in the primary CW speeds up both fast local torsional fluctuations

Table 4: Quantitative ^{1}H $T_{1\rho}$ Relaxation Times (ms) of Wild-Type *Arabidopsis* CW Polysaccharides

sites	δ_C (ppm)	*a* (rigid)	*b* (mobile)	$T_{1\rho-a}$ (ms)	$T_{1\rho-b}$ (ms)
s/iC1, GC1	105.0	0.89	0.11	18.6 ± 0.9	1.9 ± 0.4
RC1, GAC1	101.0	0.38	0.62	6.4 ± 1.2	0.9 ± 0.1
xC1, GAC1	99.3	0.50	0.50	6.0 ± 0.7	0.7 ± 0.1
iC4	88.9	1		21.3 ± 0.7	
sC4, GC4, AC4	83.5	0.73	0.27	15 ± 2	1.5 ± 0.4
RC2, GAC4	79.7	0.37	0.63	7.4 ± 0.97	0.94 ± 0.09
iC6	65.3	0.78	0.22	21.6 ± 0.8	0.92 ± 0.08
sC6, xC5	62.5	0.65	0.35	12.8 ± 0.7	1.1 ± 0.1
GC6, LC6	61.7	0.58	0.42	11.0 ± 0.7	1.10 ± 0.09

of the individual sugar units and slower cooperative motions of the polysaccharide chains.

DISCUSSION

While previous solid-state NMR studies of cellulose and cellulose−XG mixtures have been reported, these studies used ^{13}C natural-abundance material (*10*) that either precluded correlation-based definitive assignment of the ^{13}C resonances or employed site-specific ^{13}C labels (*32*) that gave only partial resonance assignment. Also, most studies did not use intact CW samples but a subset of polysaccharides extracted from the CW (*9*, *12*). The present work provides the first comprehensive analysis of the polysaccharide structures and interactions in intact primary CWs in a nearly native state by modern multidimensional solid-state NMR spectroscopy. We assigned the resonances based on the connectivity patterns, helped by literature chemical shifts (Supporting Information Table S5). The ^{13}C line widths were 1.0−2.5 ppm for cellulose, much narrower (0.4−0.9 ppm) for pectins, and intermediate (0.5−1.5 ppm) for XG. These line widths do not allow full resolution of all polysaccharide signals by 2D NMR, but the 3D CCC spectra significantly removed the congestion and clarified and confirmed many assignments. Supporting Information Table S5 shows that most of the connectivity-based assignment gave chemical shifts in agreement with the literature (within 1 ppm). The main exceptions are Rha C2 and C4 in pectin and galactose (L) C2 and C3 in XG, whose MAS chemical shifts differed from the solution NMR chemical shifts measured on extracted oligosaccharides (*30*, *33*). For Rha, whose chemical shifts are largely resolved in the 2D J-INADEQUATE spectrum, the differences likely reflect real conformational differences between the intact polysaccharides in the densely packed solid-state environment and the small oligosaccharides dissolved in solution. For Gal in XG, the solid-state chemical shifts are more overlapped with other sugar signals such as Glc in XG; thus some differences may reflect assignment uncertainties, and C4 cannot be unambiguously assigned (Supporting Information Table S5). However, the different C2 chemical shifts between our results and the literature may reflect the different XG studied: the previous sample contained a Xyl-Gal-Gal side chain (*30*) while the present *Arabidopsis* CW samples contain hemicellulosic Gal side chains either in a terminal position or with a fucose attached at C2. The C3 chemical shift difference is more puzzling and currently not completely understood. The 74.0−76.7 cross-peak so far assigned to L C2−C3 occurs in a high-intensity region of the DP-INADEQUATE spectrum (Figure 2B) and was not assigned to other sugar moieties. Finally, ambiguities exist about the assignment of GA C3 of pectin, which is not identified in the 2D INADEQUATE spectrum. On the other hand, the C4−C5−C6 connectivities are readily identified with the help of the 171 ppm C6 peak, and C1−C2 peaks are also well resolved from the signals of other mobile polysaccharides.

The intermolecular cross-peaks in the 3D ^{13}C correlation spectra gave clear constraints to the packing and interactions of the polysaccharides in primary plant CWs. Currently, the prevailing model of primary CW structure posits two distinct polysaccharide networks, one involving cellulose microfibrils cross-linked by XGs and the other involving direct pectin−hemicellulose interactions (*5*, *6*, *34*). Contrary to this model, the cross-peaks observed in the 3D NMR spectra indicate that pectins interact extensively with both cellulose and XGs, while XG−cellulose contacts are more limited than previously thought. The latter is evidenced by the absence of Xyl−cellulose cross-peaks (Figure 5B) and the low intensities of the observed XG−cellulose correlations (Figure 4 and Supporting Information Figures S4 and S5). Xyloglucan was thought to either completely coat the surface of microfibrils or intercalate into the microfibrils (*5*, *35*, *36*). The 3D spectra, which exhibit cross-peaks between interior cellulose and the XG backbone Glc and side chains (Figure 3, 4), are most consistent with partial entrapment of XGs into the cellulose microfibrils without covering a sizable fraction of the surface. Based on the similar intensities of the resolved C4 signals of the interior (89 ppm) and surface cellulose (85 ppm), the microfibril diameters in wild-type CWs are only about 3−4 nm. This small diameter is consistent with the abundance of surface−interior cellulose cross-peaks (Figure 3A) and is also in good agreement with previous X-ray scattering and 1D ^{13}C NMR spectra of other primary CWs (*37*, *38*). XG intercalation into these relatively thin microfibrils can thus affect a significant fraction of the interior cellulose, making cross-peaks between them observable. Our spectra indicate that the number of XG segments intercalated into the microfibrils is not large, thus a significant fraction of XG chains should remain in the interfibrillar space. The entrapped versus free XG domains should have distinct dynamics, consistent with the heterogeneity of the relaxation rates.

The infrequent but deep intercalation of XG into cellulose microfibrils explains the previous observation that ~15% of XG chains could not be extracted by XG-specific endoglucanase nor 4 M KOH but was only solubilized when treated with cellulase (*36*). The lack of extensive surface−cellulose to XG cross-peaks is also consistent with recent studies of XG−cellulose model composites, where ^{13}C spectral editing experiments based on ^{1}H $T_{1\rho}$ relaxation times failed to detect XG signals associated with rigid cellulose (*12*). Quantification of ^{13}C intensities in 1-^{13}C- and 4-^{13}C-labeled mung bean primary CWs also suggested that less than 10% of the surface of the cellulose microfibrils was coated with XG (*32*), in qualitative agreement with the 3D results here. However, the earlier spectral editing experiments were based on superposition of rigid and mobile polysaccharide spectra using weights that were semiquantitatively chosen. The distribution of the relaxation times measured in this work suggests that such separation of the rigid and mobile subspectra may be incomplete. In comparison, the 3D correlation approach used here provides more unambiguous proof of the presence or absence of cellulose−hemicellulose and cellulose−pectin contacts.

The CW structural model that emerges from these structural and dynamic data showcases pectins as the central polysaccharides that interact with both the cellulose microfibrils and hemicelluloses in a single network, thus revising the current

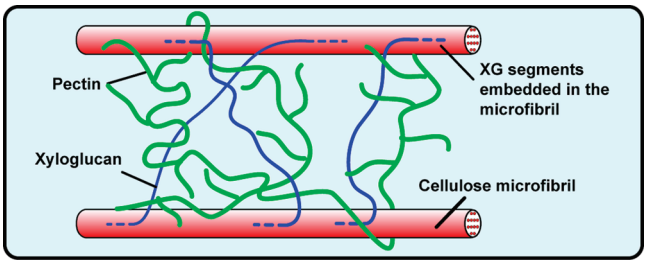

FIGURE 8: A new structural model of plant CWs. Pectins (curved green chains) exhibit numerous interactions with the surface of cellulose microfibrils (red cylinders) and with XG (blue chains) and undergo large-amplitude motions. A limited number of XG segments intercalates (dashed blue lines) into the cellulose microfibrils, endowing XG with partial rigidity and heterogeneous dynamics. All three types of polysaccharides interact in a single network.

two-network paradigm (*6*) (Figure 8). The pectins contain both highly mobile segments between microfibrils and a small fraction of more rigid domains that interact with the other polysaccharides. The heterogeneity of pectin dynamics is consistent with alkaline extraction of sugar beet walls, which yielded two fractions of pectic arabinan and galactan side chains, one with high mobility and the other with restricted mobility (*39*). The pectin−XG cross-peaks are also consistent with previous extraction analysis of the primary CWs of suspension-cultured rose cells, which suggested the presence of covalent linkages between XGs and acidic pectins (*40*). The extensive interaction of pectins with surface cellulose supports the well-known role of pectin in plant cell adhesion and control of CW porosity, by regulating the interfibrillar spacing and relative orientations of the microfibrils (*6*, *41*). Our results suggest that load bearing is shared by all three types of polysaccharides rather than by XG−cellulose alone. The microfibrils, free of hemicellulose coating, interact directly with pectins. XGs still exert rigidifying influences on the CW, as indicated by the faster motions of the polysaccharides in the XG-deficient mutant. However, the amplitudes of motion are similar in the mutant and wild-type CWs, suggesting similar polysaccharide packing densities. Thus, the significant retention of the tensile strength of the mutant CW may result from the combined effects of pectins and subtle compensatory changes of the CW structure, which include enlargement of the microfibril diameter (Figure 6A) and the increased amounts of xylan and some pectic polysaccharides (Table 1) in the CW.

This study demonstrates that ^{13}C labeling combined with MAS multidimensional correlation solid-state NMR spectroscopy can elucidate the molecular interactions of plant CWs in a near-native state. Application of this approach to the investigation of other important questions of plant CW structure can be readily envisioned: for example, glycoprotein−polysaccharide interactions and the evolution of CW structure with plant growth will now be open to molecular level studies in a native environment.

ACKNOWLEDGMENT

The authors thank Dr. Shenhui Li and Sarah D. Cady for experimental assistance.

SUPPORTING INFORMATION AVAILABLE

Pulse sequences, illustrations of assignment strategy, additional 2D and 3D spectra, tables of order parameters and relaxation times, experimental conditions, and the spectral locations of cross-peaks. This material is available free of charge via the Internet at http://pubs.acs.org.

REFERENCES

1. Somerville, C., Bauer, S., Brininstool, G., Facette, M., Hamann, T., Milne, J., Osborne, E., Paredez, A., Persson, S., Raab, T., Vorwerk, S., and Youngs, H. (2004) Toward a systems approach to understanding plant cell walls. *Science 306*, 2206–2211.
2. Talmadge, K. W., Keegstra, K., Bauer, W. D., and Albersheim, P. (1973) The structure of plant cell walls: I. The macromolecular components of the walls of suspension-cultured sycamore cells with a detailed analysis of the pectic polysaccharides. *Plant Physiol. 51*, 158–173.
3. Albersheim, P., Darvill, A., Roberts, K., Sederoff, R., and Staehelin, A. (2010) Plant Cell Walls, Garland Science, Taylor & Francis Group, LLC, New York.
4. Zablackis, E., Huang, J., Müller, B., Darvill, A. G., and Albersheim, P. (1995) Characterization of the cell-wall polysaccharides of *Arabidopsis thaliana* leaves. *Plant Physiol. 107*, 1129–1138.
5. Cosgrove, D. J. (2001) Wall structure and wall loosening. A look backwards and forwards. *Plant Physiol. 125*, 131–134.
6. Carpita, N. C., and Gibeaut, D. M. (1993) Structural models of primary cell walls in flowering plants: consistency of molecular structure with the physical properties of the walls during growth. *Plant J. 3*, 1–30.
7. Sarkar, P., Bosneaga, E., and Auer, M. (2009) Plant cell walls throughout evolution: towards a molecular understanding of their design principles. *J. Exp. Bot. 60*, 15–35.
8. Jarvis, M. C. (1992) Self-assembly of plant cell walls. *Plant, Cell Environ. 15*, 1–5.
9. Davies, L. M., Harris, P. J., and Newman, R. H. (2002) Molecular ordering of cellulose after extraction of polysaccharides from primary cell walls of *Arabidopsis thaliana*: a solid-state CP/MAS (13)C NMR study. *Carbohydr. Res. 337*, 587–593.
10. Atalla, R. H., and VanderHart, D. L. (1984) Native cellulose: a composite of two distinct crystalline forms. *Science 223*, 283–285.
11. Atalla, R. H., and Vanderhart, D. L. (1999) The role of solid state ^{13}C NMR spectroscopy in studies of the nature of native celluloses. *Solid-State Nucl. Magn. Reson. 15*, 1–19.
12. Bootten, T. J., Harris, P. J., Melton, L. D., and Newman, R. H. (2009) Solid-state (13)C NMR study of a composite of tobacco xyloglucan and *Gluconacetobacter xylinus* cellulose: molecular interactions between the component polysaccharides. *Biomacromolecules 10*, 2961–2967.
13. Bootten, T. J., Harris, P. J., Melton, L. D., and Newman, R. H. (2008) WAXS and C-13 NMR study of *Gluconoacetobacter xylinus* cellulose in composites with tamarind xyloglucan. *Carbohydr. Res. 343*, 221–229.
14. Cady, S. D., Schmidt-Rohr, K., Wang, J., Soto, C. S., DeGrado, W. F., and Hong, M. (2010) Structure of the amantadine binding site of influenza M2 proton channels in lipid bilayers. *Nature 463*, 689–692.
15. Wasmer, C., Lange, A., Van Melckebeke, H., Siemer, A. B., Riek, R., and Meier, B. H. (2008) Amyloid fibrils of the HET-s(218−289) prion form a beta solenoid with a triangular hydrophobic core. *Science 319*, 1523–1526.
16. Castellani, F., von Rossum, B. J., Diehl, A., Rehbein, K., and Oschkinat, H. (2003) Determination of solid-state NMR structures of proteins by means of three-dimensional ^{15}N-^{13}C-^{13}C dipolar correlation spectroscopy and chemical shift analysis. *Biochemistry 42*, 11476–11483.
17. Cavalier, D. M., Lerouxel, O., Neumetzler, L., Yamauchi, K., Reinecke, A., Freshour, G., Zabotina, O. A., Hahn, M. G., Burgert, I., Pauly, M., Raikhel, N. V., and Keegstra, K. (2008) Disrupting two *Arabidopsis thaliana* xylosyltransferase genes results in plants deficient in xyloglucan, a major primary cell wall component. *Plant Cell 20*, 1519–1537.
18. Zabotina, O. A., van de Ven, W. T., Freshour, G., Drakakaki, G., Cavalier, D., Mouille, G., Hahn, M. G., Keegstra, K., and Raikhel, N. V. (2008) *Arabidopsis* XXT5 gene encodes a putative alpha-1,6-xylosyltransferase that is involved in xyloglucan biosynthesis. *Plant J. 56*, 101–115.
19. Ciucanu, I. (2006) Per-O-methylation reaction for structural analysis of carbohydrates by mass spectrometry. *Anal. Chim. Acta 576*, 147–155.
20. Hohwy, M., Jakobsen, H. J., Eden, M., Levitt, M. H., and Nielsen, N. C. (1998) Broadband dipolar recoupling in the nuclear magnetic resonance of rotating solids: a compensated C7 pulse sequence. *J. Chem. Phys. 108*, 2686–2694.

21. Takegoshi, K., Nakamura, S., and Terao, T. (2001) C-13-H-1 dipolar-assisted rotational resonance in magic-angle spinning NMR. *Chem. Phys. Lett. 344*, 631–637.
22. Bax, A., Freeman, R., and Kempsell, S. P. (1980) Natural-abundance ^{13}C-^{13}C coupling observed via double-quantum coherence. *J. Am. Chem. Soc. 102*, 4849–4851.
23. Li, S., Zhang, Y., and Hong, M. (2010) 3D ^{13}C-^{13}C-^{13}C correlation NMR for de novo distance determination of solid proteins and application to a human alpha defensin. *J. Magn. Reson. 202*, 203–210.
24. Munowitz, M. G., Griffin, R. G., Bodenhausen, G., and Huang, T. H. (1981) Two-dimensional rotational spin-echo NMR in solids: correlation of chemical shift and dipolar interactions. *J. Am. Chem. Soc. 103*, 2529–2533.
25. Bielecki, A., Kolbert, A. C., de Groot, H. J. M., Griffin, R. G., and Levitt, M. H. (1990) Frequency-switched Lee-Goldburg sequences in solids. *Adv. Magn. Reson. 14*, 111–124.
26. Zabotina, O., Malm, E., Drakakaki, G., Bulone, V., and Raikhel, N. (2008) Identification and preliminary characterization of a new chemical affecting glucosyltransferase activities involved in plant cell wall biosynthesis. *Mol. Plant 1*, 977–989.
27. Pines, A., Gibby, M. G., and Waugh, J. S. (1973) Proton-enhanced NMR of dilute spins in solids. *J. Chem. Phys. 59*, 569–590.
28. Ishii, T., Ichita, J., Matsue, H., Ono, H., and Maeda, I. (2002) Fluorescent labeling of pectic oligosaccharides with 2-aminobenzamide and enzyme assay for pectin. *Carbohydr. Res. 337*, 1023–1032.
29. Habibi, Y., Mostafa, M., and Vignon, M. R. (2005) Arabinan-rich polysaccharides isolated and characterized from the endosperm of the seed of *Opuntia ficus-indica* prickly pear fruits. *Carbohydr. Polym. 60*, 319–329.
30. Hantus, S., Pauly, M., Darvill, A. G., Albersheim, P., and York, W. S. (1997) Structural characterization of novel L-galactose-containing oligosaccharide subunits of jojoba seed xyloglucans. *Carbohydr. Res. 304*, 11–20.
31. Huster, D., Xiao, L. S., and Hong, M. (2001) Solid-state NMR investigation of the dynamics of colicin Ia channel-forming domain. *Biochemistry 40*, 7662–7674.
32. Bootten, T. J., Harris, P. J., Melton, L. D., and Newman, R. H. (2004) Solid-state ^{13}C-NMR spectroscopy shows that the xyloglucans in the primary cell walls of mung bean (*Vigna radiata* L.) occur in different domains: a new model for xyloglucan-cellulose interactions in the cell wall. *J. Exp. Bot. 55*, 571–583.
33. Habibi, Y., Heyraud, A., Mahrouz, M., and Vignon, M. R. (2004) Structural features of pectic polysaccharides from the skin of *Opuntia ficus-indica* prickly pear fruits. *Carbohydr. Res. 339*, 1119–1127.
34. Keegstra, K., Talmadge, K. W., Bauer, W. D., and Albersheim, P. (1973) The structure of plant cell walls: III. A model of the walls of suspension-cultured sycamore cells based on the interconnections of the macromolecular components. *Plant Physiol. 51*, 188–197.
35. Hayashi, T., and Maclachlan, G. (1984) Pea xyloglucan and cellulose: I. Macromolecular organization. *Plant Physiol. 75*, 596–604.
36. Pauly, M., Albersheim, P., Darvill, A., and York, W. S. (1999) Molecular domains of the cellulose/xyloglucan network in the cell walls of higher plants. *Plant J. 20*, 629–639.
37. Kennedy, C. J., Cameron, G. J., Sturcova, A., Apperley, D. C., Altaner, C., Wess, T. J., and Jarvis, M. C. (2007) Microfibril diameter in celery collenchyma cellulose: X-ray scattering and NMR evidence. *Cellulose 14*, 235–246.
38. Newman, R. H. (1999) Estimation of the lateral dimensions of cellulose crystallites using ^{13}C NMR signal strengths. *Solid-State Nucl. Magn. Reson. 15*, 21–29.
39. Zykwinska, A., Rondeau-Mouro, C., Garnier, C., Thibault, J. F., and Ralet, M. C. (2006) Alkaline extractability of pectic arabinan and galactan and their mobility in sugar beet and potato cell walls. *Carbohydr. Polym. 65*, 510–520.
40. Thompson, J. E., and Fry, S. C. (2000) Evidence for covalent linkage between xyloglucan and acidic pectins in suspension-cultured rose cells. *Planta 211*, 275–286.
41. Jarvis, M. C., Briggs, S. P. H., and Knox, J. P. (2003) Intercellular adhesion and cell separation in plants. *Plant, Cell Environ. 26*, 977–989.